Identifying Environments Galaxies Reside In Using Topological and Hessian-Based Methods

Kiana Ejerito[a,b], Seri Nakamura[a,b], Sina Taamoli[c], Alexander de la Vega[c]

[a] *University of Hawaii at Manoa, 2500 Campus Rd, Honolulu, HI 96822, USA*
[b] *Institute for Astronomy, University of Hawai'i, 2680 Woodlawn Drive, Honolulu, HI 96822, USA*
[c] *University of California Riverside, 900 University Ave, Riverside, CA 92521*

Abstract

Overall, the relationship between galaxy evolution and its environment is still not well defined. Therefore, it is crucial to have faster, more robust ways of defining the environmental shape making machine learning an ideal method of environment classification. However, a labeled data set or a mask is required, which can be generated with traditional filament-finding algorithms. In this project, we use the topological algorithm, `DisPerSE` to create a catalog of filaments in COSMOS2020 using reconstructed density fields. We find that `DisPerSE` is able to accurately detect the most prominent filaments. Additionally, it is computationally efficient in comparison to other algorithms. In the future, this catalog can be used to train a machine learning model to classify the environment shape and relate it to star formation rates and can be applied to other surveys that may be deeper and span a larger area.

Keywords:

1. Introduction

The large-scale structure of the universe can be described as a multi-scale network, known as the cosmic web as galaxies, gas, and dark matter are distributed in dense clusters, filaments, sheet-like walls, and empty, "void" regions (Bond et al., 1996). The study of the cosmic web is crucial to test our cosmological models, gravity, and general relativity.

To understand galaxy evolution, we can relate properties such as star formation rates (SFRs) of galaxies to their environment. At low redshifts ($z \lessapprox 1$), there is a well-established anticorrelation between SFRs and overdensities (Patel et al., 2009). However, at higher redshifts, there are predictions that these relationships lessen (Grützbauch et al., 2011; Scoville et al., 2013; Darvish et al., 2016) or reverse (Lemaux et al., 2022). Additionally, the environment is predicted to influence the morphology and orientation of galaxies. Thus, there is a need to classify densities and environment shape across a broad range of redshifts.

New methods such as machine learning are a faster way to determine the environmental shape. Aragon-Calvo (2019) introduces the use of convolutional neural network (CNN) model U-Net trained on Voronoi models and N-body simulations. Other astronomical fields

have used Mask R-CNN methods to detect solar or ISM filaments (Salasa and Arymurthy, 2019; Alina et al., 2022).

A challenging part of using these machine learning techniques is the requirement of creating labeled datasets or masks. However, it is difficult to identify different components of cosmic web, as they are not well-defined structures due to their multiscale nature and complex shapes. There have been many attempts in the literature to identify cosmic filaments and understand their properties. In terms of simulations, many different filament algorithms have been developed and tested with several types of simulations. Galárraga-Espinosa et al. (2022) and Galárraga-Espinosa et al. (2024) both use the `DisPerSE` code to identify filaments in the IllustrisTNG and MTNG simulations, respectively, and observe the properties and evolution of these filaments. Additionally, Libeskind et al. (2018) compares multiple ways of identifying filaments in observational and simulated datasets. Percolation and graphing techniques use a minimum spanning tree of galaxy distribution to identify filaments (Alpaslan et al., 2014). Stochastic methods of geometric configurations, such as Bisous models are useful because they only require coordinates of the galaxy haloes (Tempel et al., 2016; Stoica et al., 2010), but are computationally demanding. Hessian-based methods are a common way to classify the environment shape, taking the Hessian matrix of the density, tidal, or velocity shear fields and defining the environment by its eigenvalues (Aragón-Calvo et al., 2007; Hahn et al., 2007; Forero-Romero et al., 2009; Bond et al., 2010; Libeskind et al., 2012; Cautun et al., 2013; Pfeifer et al., 2022). Topological models, such as `Spineweb` (Aragón-Calvo et al., 2010) and `DisPerSE` (Sousbie et al., 2011) use ideas of the Morse theory to look at the density field and its gradient to find critical points and define lines connecting these points to detect filaments. Phase-space methods looks at the evolving spatial mass distribution, appearing as a 2D sheet folding itself in 6D phase space, such as the ORIGAMI formalism (Falck et al., 2012; Falck and Neyrinck, 2015).

Additionally, with the improvement in large-scale, deep surveys, photometric and spectroscopic redshifts can also be used to trace the cosmic web and understand these filametary structures. The cosmic web of galaxies has been observed with surveys such as the Sloan Digital Sky Survey (SDSS, (York et al., 2000)), two degree Field Galaxy Redshift Survey (2dFGRS, (Colless et al., 2003)), the 2MASS redshift survey (Huchra et al., 2012), VIPERS (Guzzo et al., 2014), the SAMI survey (Bryant et al., 2015), COSMOS2015 (Laigle et al., 2018) and more.

Taamoli et al. (2024) uses COSMOS2020 data to estimate the environmental density and relate this to star formation rates. In this project, we expand on the work of Taamoli et al. (2024) to identify cosmic filaments using DisPersE (Sousbie et al., 2011) from the density maps and create a labeled dataset to train a machine learning model.

2. Methodology

2.1. COSMOS2020 Catalog and Density Maps

The data and density maps are detailed in Taamoli et al. (2024), and briefly outlined in this paper. COSMOS2020 includes approximately 1.7 million sources across $\sim 2\,\mathrm{deg}^2$ COSMOS field. The COSMOS2020 data catalogs we use are constructed with `The Farmer`

(Weaver et al., 2023), a profile-fitting photometric tool based on `The Tractor` (Lang et al., 2016). `The Tractor` fits galaxy brightness profiles to derive photometry, in which `The Tractor` uses a decision tree to find the best-fit model. Additionally, we use COSMOS2020 data analyzed with the `LePhare` spectral energy distribution fitting code (Arnouts et al., 2002) to fit galaxy and stellar templates to the observed photometry. The final sample included 211,431 galaxies in a photo-z range of $0.4 < z < 6$ and have a magnitude cut of $K_s < 24.5$.

Density fields are generated for 135 redshift slices across the entire redshift range using weighted kernel density estimations (wKDE method) as seen in Chartab et al. (2020). To create these density fields, the following procedure is implemented:

1. Choose redshift slices of constant comoving width $\Delta\chi = 35h^{-1}$Mpc.
2. Calculate the weights for every galaxy in each redshift slice. A Gaussian probability distribution is assumed for each galaxy to find the weights, which is defined as the probability of a galaxy being in a redshift slice.
3. Improve the density estimation around the masked regions by applying corrections by populating them with uniformly distributed artificial sources.
4. Find the optimum bandwidth in each redshift slice, using likelihood cross-validation method, that represents the scale at the kernel smooths the density field.
5. Apply corrections for the "edge effect," which describes how the wKDE method underestimates the density near the edges of the field. In this paper, they do this correction using the renormalization method (Jones, 1993).

2.2. DisPerSE

We use the Discrete Persistent Structures Extractor, `DisPerSE`, a topological algorithm that uses Discrete Morse Theory (Forman, 2002), to identify filaments (Sousbie, 2011; Sousbie et al., 2011). Morse Theory relates the gradient of a field found from discrete data points, and the topology of the manifold and gradient to one another for smooth function. It is a well-used algorithm that can be applied to any discrete dataset, including N-body simulations and galaxy catalogs with the only constraint that a distribution must be defined over a manifold. `DisPerSE` is also versatile and can be used to detect general filamentary structures, such as molecular filaments (Arzoumanian et al., 2019).

A Delaunay tessellation field estimator (`delaunay` function) is first applied to the discrete dataset to estimate the underlying density field. `DisPerSE` then finds the critical points of the density field, where the gradient of the field is null. In 2D, the the minima, saddle points, and maxima are assigned values of 0, 1, and 2, respectively. `DisPerSE` connects the integral lines of the maxima to saddle points to identify filaments (Sousbie et al., 2011) using the `mse` function. To determine the robustness of a local topological feature such as a filament, the persistence is measured. The `skelconv` function is then used to convert the output of `mse` into a readable format and optimize the appearance of the filament output.

In this work, we immediately apply the `mse` function given the COSMOS2020 density fields. We set `-periodicity` $= 0$ for non-periodic boundaries, as the periodic boundaries are only applicable to grid type networks. The `cut` feature sets the persistence threshold,

which can estimated with the interactive `pdview` feature. Additionally, the `-cut` value can be set to the estimated amplitude of the noise. In this work, we set the cut value as the median of the density field in each redshift slice.

Then, we run the `skelconv` function, with the parameters: `-smooth` 3, `-breakdown`, and `-assemble` median 0. The `-smooth` function smooths the filament skeleton N times while keeping the critical points fixed. The `-breakdown` function merges overlapping filaments, and `-assemble` assembles arcs into longer filaments that are above a given detection threshold and do not form an angle larger than θ, expressed in degrees. We set the threshold as one sigma above the median of the density field, rounded down to the nearest tenth, and the angle as $\theta = 0$. If the estimated assemble value is around a tenths value (eg. 1.501), we round it down to the next nearest tenth to ensure the assemble threshold does not cut out an excess amount of filaments. We note that when assembling the arcs, the output filaments are very sensitive to the threshold, but not the angle as seen in Figure 1.

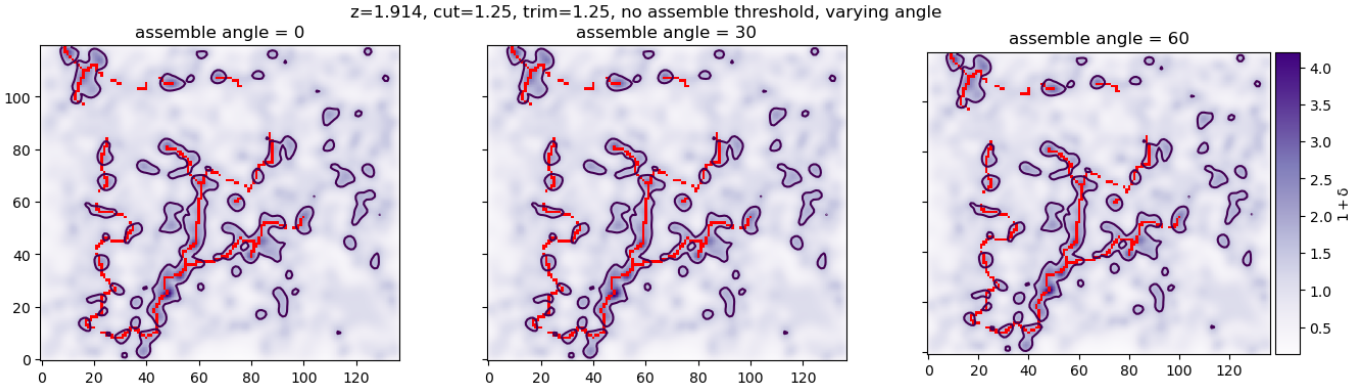

Figure 1: Filaments detected with `DisPerSE` on redshift slice $z = 1.914$ with a `cut` $= 1$ and `assemble` $= 1.25$, with varying `assemble` angels. As the angles vary, there is no visible change in the detected filaments.

3. Preliminary Results and Discussion

3.1. Detection and Performance at Varying Redshifts

`DisPerSE` was run across 135 redshift slices ranging $0.4 < z < 6$. `DisPerSE` successfully detects filamentary structures found in previous literature in the COSMOS2020 field. Iovino et al. (2016) found a long filamentary structure known as the "COSMOS Wall" composed of 1277 galaxies at $z \approx 0.73$, which is detected in our density field with `DisPerSE` in Fig 2. Casey et al. (2015) also detected an asymmetric filament at $z = 2.47$ containing 5 AGN and 7 starbursting galaxies. Fig 1 shows that at median redshift slice of $z = 2.474$, the general structure of the filament is visible, but `DisPerSE` detects more of the filamentary structure in $z = 2.516$. This could be due to the `- assemble` threshold being too close to the average overdensity value.

We note that the reliability of the reconstructed density field reduces at $z \approx 4.5$ due to the sparsity of sources and bias toward brighter objects. However, a general filamentary structure is detected in over-dense regions as seen in 4.

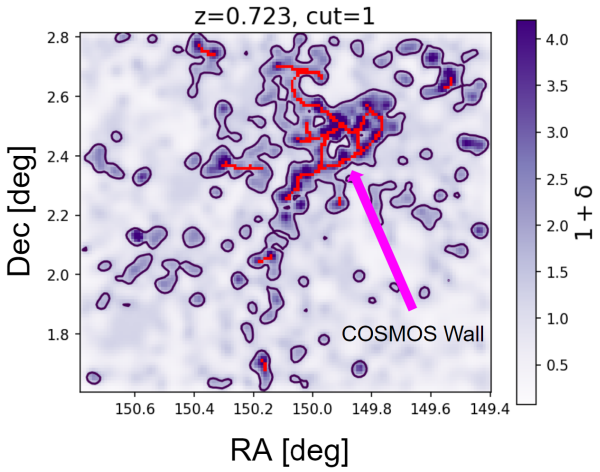

Figure 2: Long filamentary structure known as the COSMOS Wall is detected with `DisPerSE` and is in good agreement with Iovino et al. (2016).

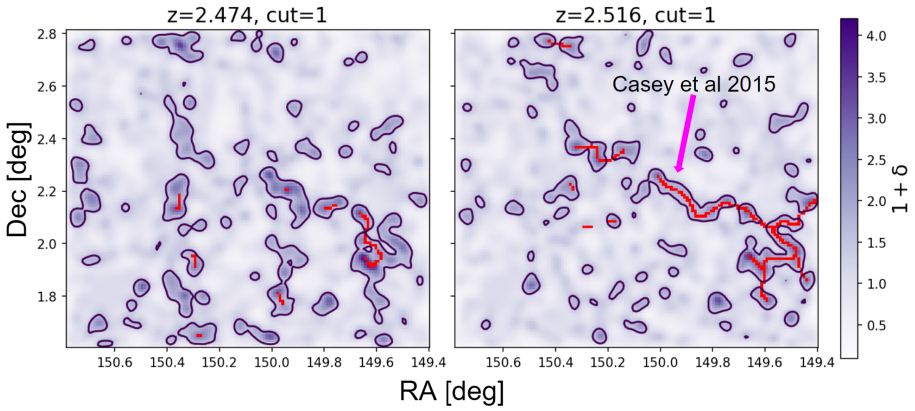

Figure 3: Filamentary structure found in Casey et al. (2015) detected with `DisPerSE` at redshift slices $z = 2.474$ and $z = 2.516$. While the general structure of the filament is present at $z = 2.474$, `DisPerSE` detects a longer structure at $z = 2.516$.

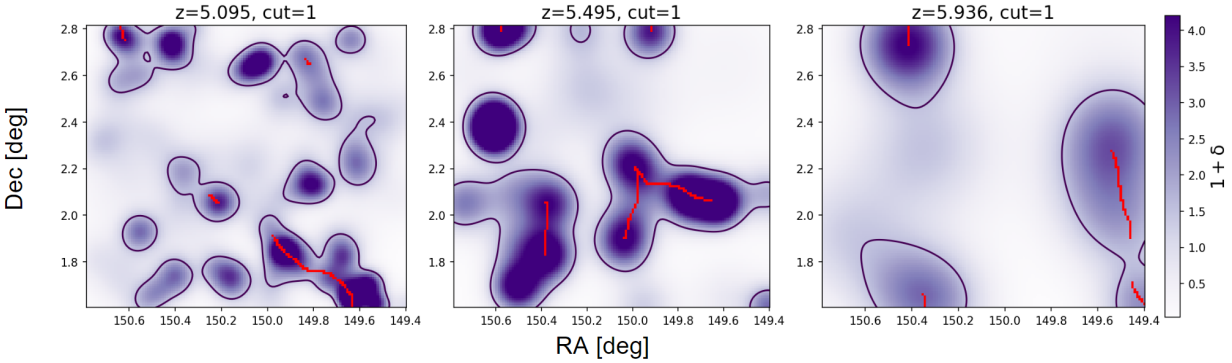

Figure 4: Filament detection at high redshifts $5 < z < 6$. The density field is much less defined in comparison to the density fields at lower redshifts due to the smaller number of sources and observational bias. However, `DisPerSE` can still detect the general over-dense regions in the field.

3.2. Performance Compared to SCONCES SCMS

The efficiency of `DisPerSE` was also compared compared to another open-sourced algorithm, `SCONCE SCMS` (`SCONCE`) (Zhang et al., 2022). We note that while there are many other algorithms that many be more well-used than `SCONCE` , they are not open-sourced or the input is not compatible with our data.

The Spherical and Conic Cosmic Web Finder `SCONCE` generalizes the subspace constrained mean shift method (SCMS). SCMS is an iterative, non-parametric estimator. `SCONCE` uses any discrete data set, weighted or unweighted, and a smoothing bandwidth and threshold. The threshold is applied to remove points farthest from the dense regions. A larger smoothing bandwidth generates a smoother kernel and "less intricate" density ridge. The underlying density field is estimated with a kernel density estimator (KDE), similarly to the density fields generated by Taamoli et al. (2024). The density ride then is defined using the Riemannian Hessian Matrix. To detect filaments, `SCONCE` iteratively computes the Hessian Matrix of the density field and the eigenvalues. The filament density ridge is then represented as a set of converged points.

To apply `SCONCE` to our data, we input the discrete dataset of galaxies weighted by their photo-z probability, in which `SCONCE` generates its own density field in comparison to inputting density fields from Taamoli et al. (2024) to `DisPerSE` . We then compare the performance of `DisPerSE` versus `SCONCE` as seen in 5. Both algorithms seem to detect the longest filamentary structure, but `SCONCE` does not detect the connecting filament at RA = 150 deg. This may indicate the optimal parameters of `SCONCE` may not be as sensitive to over-dense regions in comparison to `DisPerSE` . Computationally, `DisPerSE` is more efficient, with the filament skeleton generated in a few seconds in comparison to `SCONCE`, which can take 2-5 minutes for a single redshift slice.

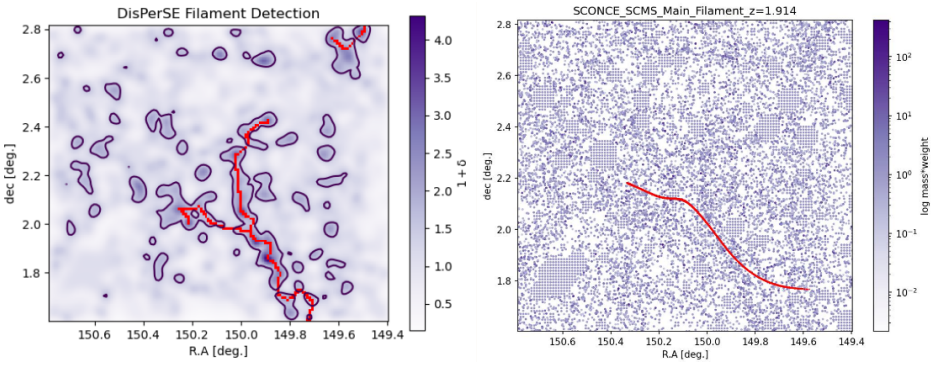

Figure 5: Filament detection of `DisPerSE` in comparison to `SCONCE` for a single redshift slice z = 1.914. Both algorithms detect the longest filamentary structure. However, `DisPerSE` detects another significant filament near approximately RA = 150.0 degrees.

4. Conclusions

Overall, the relationship between galaxy evolution and its environment is still under ongoing debate, especially at higher redshifts. Previous studies find relationships between the

environmental density and shape to galactic properties such as morphology, orientation, and SFRs. Therefore, it is crucial to have faster, more robust ways of defining the environmental shape.

It is difficult to classify the environmental shape due to its multi-scale nature in which machine learning methods may be faster and more efficient in comparison to traditional methods on large datasets but must be trained on a labeled dataset or a mask. Thus, in this paper, we use a traditional topological algorithm, `DisPerSE`, to create labels of filaments to train on machine learning algorithms. `DisPerSE` is well-used in detecting cosmic filaments and can be applied to other filamentary structures, such as molecular filaments.

We apply `DisPerSE` on the density fields of 135 redshift slices from COSMOS2020. After optimizing the `-cut` and `-assemble` values, `DisPerSE` is generally able to detect the longest filament. The accuracy of the reconstructed density field diminishes at $z \geq 4.5$, making it more difficult for `DisPerSE` to detect filaments at these redshifts. However, at slices $z \geq 4.5$, `DisPerSE` can detect general filaments in overdense regions. `DisPerSE` is also computationally efficient, taking a few seconds per redshift slice in comparison to `SCONCES SCMS`, which can take 2-5 minutes for a single slice.

In the future, we can use the catalog of filaments as a mask or labeled data set to apply to a machine learning algorithm. After classifying the environmental shape of COSMOS2020, we can relate the shape to star formation activity as proposed in Taamoli et al. (2024). Additionally, the machine learning algorithm can be used to classify environments in wider, deeper fields such as Euclid or the Hawaii Twenty Square Degree (H20) Survey to minimize cosmic variance and provide a more complete sample.

Acknowledgements

We would like to acknowledge the NSF Grant to fund the California Hawaii Astronomy Mentorship Program. We would like to thank everyone who organized the program, including director Christopher Storfer, Grey Murphree for their guidance, Bahram Mobasher, and David Sanders.

References

D. Alina, A. Shomanov, and S. Baimukhametova. MaLeFiSenta: Machine Learning for FilamentS Identification and Orientation in the ISM. *IEEE Access*, 10:74472–74482, Jan. 2022. doi: 10.1109/ACCESS.2022.3189646.

M. Alpaslan, A. S. G. Robotham, D. Obreschkow, S. Penny, S. Driver, P. Norberg, S. Brough, M. Brown, M. Cluver, B. Holwerda, A. M. Hopkins, E. van Kampen, L. S. Kelvin, M. A. Lara-Lopez, J. Liske, J. Loveday, S. Mahajan, and K. Pimbblet. Galaxy and Mass Assembly (GAMA): fine filaments of galaxies detected within voids. MNRAS, 440:L106–L110, May 2014. doi: 10.1093/mnrasl/slu019.

M. A. Aragon-Calvo. Classifying the large-scale structure of the universe with deep neural networks. MNRAS, 484(4):5771–5784, Apr. 2019. doi: 10.1093/mnras/stz393.

M. A. Aragón-Calvo, B. J. T. Jones, R. van de Weygaert, and J. M. van der Hulst. The multiscale morphology filter: identifying and extracting spatial patterns in the galaxy distribution. A&A, 474(1):315–338, Oct. 2007. doi: 10.1051/0004-6361:20077880.

M. A. Aragón-Calvo, E. Platen, R. van de Weygaert, and A. S. Szalay. The Spine of the Cosmic Web. ApJ, 723(1):364–382, Nov. 2010. doi: 10.1088/0004-637X/723/1/364.

S. Arnouts, L. Moscardini, E. Vanzella, S. Colombi, S. Cristiani, A. Fontana, E. Giallongo, S. Matarrese, and P. Saracco. Measuring the redshift evolution of clustering: the Hubble Deep Field South. MNRAS, 329(2):355–366, Jan. 2002. doi: 10.1046/j.1365-8711.2002.04988.x.

D. Arzoumanian, P. André, V. Könyves, P. Palmeirim, A. Roy, N. Schneider, M. Benedettini, P. Didelon, J. Di Francesco, J. Kirk, and B. Ladjelate. Characterizing the properties of nearby molecular filaments observed with Herschel. A&A, 621:A42, Jan. 2019. doi: 10.1051/0004-6361/201832725.

J. R. Bond, L. Kofman, and D. Pogosyan. How filaments of galaxies are woven into the cosmic web. Nature, 380(6575):603–606, Apr. 1996. doi: 10.1038/380603a0.

N. A. Bond, M. A. Strauss, and R. Cen. Crawling the cosmic network: exploring the morphology of structure in the galaxy distribution. MNRAS, 406(3):1609–1628, Aug. 2010. doi: 10.1111/j.1365-2966.2010.16823.x.

J. J. Bryant, M. S. Owers, A. S. G. Robotham, S. M. Croom, S. P. Driver, M. J. Drinkwater, N. P. F. Lorente, L. Cortese, N. Scott, M. Colless, A. Schaefer, E. N. Taylor, I. S. Konstantopoulos, J. T. Allen, I. Baldry, L. Barnes, A. E. Bauer, J. Bland-Hawthorn, J. V. Bloom, A. M. Brooks, S. Brough, G. Cecil, W. Couch, D. Croton, R. Davies, S. Ellis, L. M. R. Fogarty, C. Foster, K. Glazebrook, M. Goodwin, A. Green, M. L. Gunawardhana, E. Hampton, I. T. Ho, A. M. Hopkins, L. Kewley, J. S. Lawrence, S. G. Leon-Saval, S. Leslie, R. McElroy, G. Lewis, J. Liske, Á. R. López-Sánchez, S. Mahajan, A. M. Medling, N. Metcalfe, M. Meyer, J. Mould, D. Obreschkow, S. O'Toole, M. Pracy, S. N. Richards, T. Shanks, R. Sharp, S. M. Sweet, A. D. Thomas, C. Tonini, and C. J. Walcher. The SAMI Galaxy Survey: instrument specification and target selection. MNRAS, 447(3):2857–2879, Mar. 2015. doi: 10.1093/mnras/stu2635.

C. M. Casey, A. Cooray, P. Capak, H. Fu, K. Kovac, S. Lilly, D. B. Sanders, N. Z. Scoville, and E. Treister. A Massive, Distant Proto-cluster at z = 2.47 Caught in a Phase of Rapid Formation? ApJ, 808(2):L33, Aug. 2015. doi: 10.1088/2041-8205/808/2/L33.

M. Cautun, R. van de Weygaert, and B. J. T. Jones. NEXUS: tracing the cosmic web connection. MNRAS, 429(2):1286–1308, Feb. 2013. doi: 10.1093/mnras/sts416.

N. Chartab, B. Mobasher, B. Darvish, S. Finkelstein, Y. Guo, D. Kodra, K.-S. Lee, J. A. Newman, C. Pacifici, C. Papovich, Z. Sattari, A. Shahidi, M. E. Dickinson, S. M. Faber, H. C. Ferguson, M. Giavalisco, and M. Jafariyazani. Large-scale Structures in the CANDELS Fields: The Role of the Environment in Star Formation Activity. ApJ, 890(1):7, Feb. 2020. doi: 10.3847/1538-4357/ab61fd.

M. Colless, B. A. Peterson, C. Jackson, J. A. Peacock, S. Cole, P. Norberg, I. K. Baldry, C. M. Baugh, J. Bland-Hawthorn, T. Bridges, R. Cannon, C. Collins, W. Couch, N. Cross, G. Dalton, R. De Propris, S. P. Driver, G. Efstathiou, R. S. Ellis, C. S. Frenk, K. Glazebrook, O. Lahav, I. Lewis, S. Lumsden, S. Maddox, D. Madgwick, W. Sutherland, and K. Taylor. The 2dF Galaxy Redshift Survey: Final Data Release. *arXiv e-prints*, art. astro-ph/0306581, June 2003. doi: 10.48550/arXiv.astro-ph/0306581.

B. Darvish, B. Mobasher, D. Sobral, A. Rettura, N. Scoville, A. Faisst, and P. Capak. The Effects of the Local Environment and Stellar Mass on Galaxy Quenching to z $\sim$ 3. ApJ, 825(2):113, July 2016. doi: 10.3847/0004-637X/825/2/113.

B. Falck and M. C. Neyrinck. The persistent percolation of single-stream voids. MNRAS, 450(3):3239–3253, July 2015. doi: 10.1093/mnras/stv879.

B. L. Falck, M. C. Neyrinck, and A. S. Szalay. ORIGAMI: Delineating Halos Using Phase-space Folds. ApJ, 754(2):126, Aug. 2012. doi: 10.1088/0004-637X/754/2/126.

J. E. Forero-Romero, Y. Hoffman, S. Gottlöber, A. Klypin, and G. Yepes. A dynamical classification of the cosmic web. MNRAS, 396(3):1815–1824, July 2009. doi: 10.1111/j.1365-2966.2009.14885.x.

R. Forman. A user's guide to discrete morse theory. *Séminaire Lotharingien de Combinatoire [electronic only]*, 48:B48c–35, 2002.

D. Galárraga-Espinosa, M. Langer, and N. Aghanim. Relative distribution of dark matter, gas, and stars around cosmic filaments in the IllustrisTNG simulation. A&A, 661:A115, May 2022. doi: 10.1051/0004-6361/202141974.

D. Galárraga-Espinosa, C. Cadiou, C. Gouin, S. D. M. White, V. Springel, R. Pakmor, B. Hadzhiyska, S. Bose, F. Ferlito, L. Hernquist, R. Kannan, M. Barrera, A. Maria Delgado, and C. Hernández-Aguayo. Evolution of cosmic filaments in the MTNG simulation. A&A, 684:A63, Apr. 2024. doi: 10.1051/0004-6361/202347982.

R. Grützbauch, C. J. Conselice, A. E. Bauer, A. F. L. Bluck, R. W. Chuter, F. Buitrago, A. Mortlock, T. Weinzirl, and S. Jogee. The relationship between star formation rates, local density and stellar mass up to z $\sim$ 3 in the GOODS NICMOS Survey. MNRAS, 418(2):938–948, Dec. 2011. doi: 10.1111/j.1365-2966.2011.19559.x.

L. Guzzo, M. Scodeggio, B. Garilli, B. R. Granett, A. Fritz, U. Abbas, C. Adami, S. Arnouts, J. Bel, M. Bolzonella, D. Bottini, E. Branchini, A. Cappi, J. Coupon, O. Cucciati, I. Davidzon, G. De Lucia, S. de la Torre, P. Franzetti, M. Fumana, P. Hudelot, O. Ilbert, A. Iovino, J. Krywult, V. Le Brun, O. Le Fèvre, D. Maccagni, K. Małek, F. Marulli, H. J. McCracken, L. Paioro, J. A. Peacock, M. Polletta, A. Pollo, H. Schlagenhaufer, L. A. M. Tasca, R. Tojeiro, D. Vergani, G. Zamorani, A. Zanichelli, A. Burden, C. Di Porto, A. Marchetti, C. Marinoni, Y. Mellier, L. Moscardini, R. C. Nichol, W. J. Percival, S. Phleps, and M. Wolk. The VIMOS Public Extragalactic Redshift Survey (VIPERS). An unprecedented view of galaxies and large-scale structure at 0.5 ¡ z ¡ 1.2. A&A, 566:A108, June 2014. doi: 10.1051/0004-6361/201321489.

O. Hahn, C. Porciani, C. M. Carollo, and A. Dekel. Properties of dark matter haloes in clusters, filaments, sheets and voids. MNRAS, 375(2):489–499, Feb. 2007. doi: 10.1111/j.1365-2966.2006.11318.x.

J. P. Huchra, L. M. Macri, K. L. Masters, T. H. Jarrett, P. Berlind, M. Calkins, A. C. Crook, R. Cutri, P. Erdoğdu, E. Falco, T. George, C. M. Hutcheson, O. Lahav, J. Mader, J. D. Mink, N. Martimbeau, S. Schneider, M. Skrutskie, S. Tokarz, and M. Westover. The 2MASS Redshift Survey—Description and Data Release. ApJS, 199(2):26, Apr. 2012. doi: 10.1088/0067-0049/199/2/26.

A. Iovino, V. Petropoulou, M. Scodeggio, M. Bolzonella, G. Zamorani, S. Bardelli, O. Cucciati, L. Pozzetti, L. Tasca, D. Vergani, E. Zucca, A. Finoguenov, O. Ilbert, M. Tanaka, M. Salvato, K. Kovač, and P. Cassata. A high definition view of the COSMOS Wall at z ~0.73. A&A, 592:A78, Aug. 2016. doi: 10.1051/0004-6361/201527673.

M. C. Jones. Simple boundary correction for kernel density estimation. *Statistics and computing*, 3:135–146, 1993.

C. Laigle, C. Pichon, S. Arnouts, H. J. McCracken, Y. Dubois, J. Devriendt, A. Slyz, D. Le Borgne, A. Benoit-Lévy, H. S. Hwang, O. Ilbert, K. Kraljic, N. Malavasi, C. Park, and D. Vibert. COSMOS2015 photometric redshifts probe the impact of filaments on galaxy properties. MNRAS, 474(4):5437–5458, Mar. 2018. doi: 10.1093/mnras/stx3055.

D. Lang, D. W. Hogg, and D. Mykytyn. The Tractor: Probabilistic astronomical source detection and measurement. Astrophysics Source Code Library, record ascl:1604.008, Apr. 2016.

B. C. Lemaux, O. Cucciati, O. Le Fèvre, G. Zamorani, L. M. Lubin, N. Hathi, O. Ilbert, D. Pelliccia, R. Amorín, S. Bardelli, P. Cassata, R. R. Gal, B. Garilli, L. Guaita, M. Giavalisco, D. Hung, A. Koekemoer, D. Maccagni, L. Pentericci, B. Ribeiro, D. Schaerer, E. Shah, L. Shen, P. Staab, M. Talia, R. Thomas, A. R. Tomczak, L. Tresse, E. Vanzella, D. Vergani, and E. Zucca. The VIMOS Ultra Deep Survey: The reversal of the star-formation rate − density relation at 2 ¡ z ¡ 5. A&A, 662:A33, June 2022. doi: 10.1051/0004-6361/202039346.

N. I. Libeskind, Y. Hoffman, A. Knebe, M. Steinmetz, S. Gottlöber, O. Metuki, and G. Yepes. The cosmic web and the orientation of angular momenta. MNRAS, 421(1):L137–L141, Mar. 2012. doi: 10.1111/j.1745-3933.2012.01222.x.

N. I. Libeskind, R. van de Weygaert, M. Cautun, B. Falck, E. Tempel, T. Abel, M. Alpaslan, M. A. Aragón-Calvo, J. E. Forero-Romero, R. Gonzalez, S. Gottlöber, O. Hahn, W. A. Hellwing, Y. Hoffman, B. J. T. Jones, F. Kitaura, A. Knebe, S. Manti, M. Neyrinck, S. E. Nuza, N. Padilla, E. Platen, N. Ramachandra, A. Robotham, E. Saar, S. Shandarin, M. Steinmetz, R. S. Stoica, T. Sousbie, and G. Yepes. Tracing the cosmic web. MNRAS, 473(1):1195–1217, Jan. 2018. doi: 10.1093/mnras/stx1976.

S. G. Patel, B. P. Holden, D. D. Kelson, G. D. Illingworth, and M. Franx. The Dependence of Star Formation Rates on Stellar Mass and Environment at z ~0.8. ApJ, 705(1):L67–L70, Nov. 2009. doi: 10.1088/0004-637X/705/1/L67.

S. Pfeifer, N. I. Libeskind, Y. Hoffman, W. A. Hellwing, M. Bilicki, and K. Naidoo. COWS: a filament finder for Hessian cosmic web identifiers. MNRAS, 514(1):470–479, July 2022. doi: 10.1093/mnras/stac1382.

R. P. Salasa and A. M. Arymurthy. Solar filament detection using mask r-cnn. In *2019 International Workshop on Big Data and Information Security (IWBIS)*, pages 67–71, 2019. doi: 10.1109/IWBIS.2019.8935810.

N. Scoville, S. Arnouts, H. Aussel, A. Benson, A. Bongiorno, K. Bundy, M. A. A. Calvo, P. Capak, M. Carollo, F. Civano, J. Dunlop, M. Elvis, A. Faisst, A. Finoguenov, H. Fu, M. Giavalisco, Q. Guo, O. Ilbert, A. Iovino, M. Kajisawa, J. Kartaltepe, A. Leauthaud, O. Le Fèvre, E. LeFloch, S. J. Lilly, C. T. C. Liu, S. Manohar, R. Massey, D. Masters, H. J. McCracken, B. Mobasher, Y. J. Peng, A. Renzini, J. Rhodes, M. Salvato, D. B. Sanders, B. D. Sarvestani, C. Scarlata, E. Schinnerer, K. Sheth, P. L. Shopbell, V. Smolčić, Y. Taniguchi, J. E. Taylor, S. D. M. White, and L. Yan. Evolution of Galaxies and Their Environments at z = 0.1-3 in COSMOS. ApJS, 206(1):3, May 2013. doi: 10.1088/0067-0049/206/1/3.

T. Sousbie. The persistent cosmic web and its filamentary structure - I. Theory and implementation. MNRAS, 414(1):350–383, June 2011. doi: 10.1111/j.1365-2966.2011.18394.x.

T. Sousbie, C. Pichon, and H. Kawahara. The persistent cosmic web and its filamentary structure - II. Illustrations. MNRAS, 414(1):384–403, June 2011. doi: 10.1111/j.1365-2966.2011.18395.x.

R. S. Stoica, V. J. Martínez, and E. Saar. Filaments in observed and mock galaxy catalogues. A&A, 510: A38, Feb. 2010. doi: 10.1051/0004-6361/200912823.

S. Taamoli, B. Mobasher, N. Chartab, B. Darvish, J. R. Weaver, S. Hemmati, C. M. Casey, Z. Sattari, G. Brammer, P. L. Capak, O. Ilbert, J. S. Kartaltepe, H. J. McCracken, A. Moneti, D. B. Sanders, N. Scoville, C. L. Steinhardt, and S. Toft. Large-scale Structures in COSMOS2020: Evolution of Star Formation Activity in Different Environments at 0.4 ¡ z ¡ 4. ApJ, 966(1):18, May 2024. doi: 10.3847/1538-4357/ad32c5.

E. Tempel, R. S. Stoica, R. Kipper, and E. Saar. Bisous model-Detecting filamentary patterns in point processes. *Astronomy and Computing*, 16:17–25, July 2016. doi: 10.1016/j.ascom.2016.03.004.

J. R. Weaver, L. Zalesky, V. Kokorev, C. J. R. McPartland, N. Chartab, K. M. L. Gould, M. Shuntov, I. Davidzon, A. Faisst, N. Stickley, P. L. Capak, S. Toft, D. Masters, B. Mobasher, D. B. Sanders, O. B. Kauffmann, H. J. McCracken, O. Ilbert, G. Brammer, and A. Moneti. The Farmer: A Reproducible Profile-fitting Photometry Package for Deep Galaxy Surveys. ApJS, 269(1):20, Nov. 2023. doi: 10.3847/1538-4365/acf850.

D. G. York, J. Adelman, J. Anderson, John E., and S. F. Anderson. The Sloan Digital Sky Survey: Technical Summary. AJ, 120(3):1579–1587, Sept. 2000. doi: 10.1086/301513.

Y. Zhang, R. S. de Souza, and Y.-C. Chen. SCONCE: a cosmic web finder for spherical and conic geometries. MNRAS, 517(1):1197–1217, Nov. 2022. doi: 10.1093/mnras/stac2504.